



UNIVERSITY OF LEEDS

This is a repository copy of *Elastic and inelastic buckling of steel cellular beams under strong-axis bending*.

White Rose Research Online URL for this paper:
<https://eprints.whiterose.ac.uk/165162/>

Version: Accepted Version

Article:

Rajana, K, Tsavdaridis, KD orcid.org/0000-0001-8349-3979 and Koltsakis, E (2020) Elastic and inelastic buckling of steel cellular beams under strong-axis bending. *Thin-Walled Structures*, 156. 106955. ISSN 0263-8231

<https://doi.org/10.1016/j.tws.2020.106955>

© 2020, Elsevier. This manuscript version is made available under the CC-BY-NC-ND 4.0 license <http://creativecommons.org/licenses/by-nc-nd/4.0/>.

Reuse

This article is distributed under the terms of the Creative Commons Attribution-NonCommercial-NoDerivs (CC BY-NC-ND) licence. This licence only allows you to download this work and share it with others as long as you credit the authors, but you can't change the article in any way or use it commercially. More information and the full terms of the licence here: <https://creativecommons.org/licenses/>

Takedown

If you consider content in White Rose Research Online to be in breach of UK law, please notify us by emailing eprints@whiterose.ac.uk including the URL of the record and the reason for the withdrawal request.



eprints@whiterose.ac.uk
<https://eprints.whiterose.ac.uk/>

Elastic and Inelastic Buckling of Steel Cellular Beams under Strong-Axis Bending

Komal Rajana¹, Konstantinos Daniel Tsavdaridis^{2*} and Efthymios Koltsakis³

¹PhD Student, School of Mathematics, Computer Science and Engineering, Civil Engineering, City,
University of London, EC1V 0HB, London, UK

²Associate Professor of Structural Engineering, School of Civil Engineering, Faculty of Engineering and
Physical Sciences, University of Leeds, LS2 9JT, Leeds, UK

³Associate Professor, Department of Civil Engineering, Aristotle University of Thessaloniki, Greece

**Corresponding author, E-mail: K.Tsavdaridis@leeds.ac.uk*

ABSTRACT

This paper presents an extensive parametric study of elastic and inelastic buckling of cellular beams subjected to strong axis bending in order to investigate the effect of a variety of geometric parameters, and further generate mass data to validate and train a neural network-based formula. Python was employed to automate mass finite element (FE) analyses and reliably examine the influence of the parameters. Overall, 102,060 FE analyses were performed. The effects of the initial geometric imperfection, material nonlinearity, manufacture-introduced residual stresses, web opening diameter, web-post width, web height, flange width, web and flange thickness, end web-post width, and span of the beams and their combinations were thoroughly examined. The results are also compared with the current state-of-the-art design guidelines used in the UK.

It was concluded that the critical elastic buckling load of perforated beams corresponds to the lateral movement of the compression flange while the most critical parameters are the web thickness and the geometry of the flange. However, from the inelastic analysis, the geometry and position of the web opening influence the collapse load capacity in a similar fashion to the geometry of the flange and thickness of the web. It was also concluded that the effect of the initial conditions was insignificant.

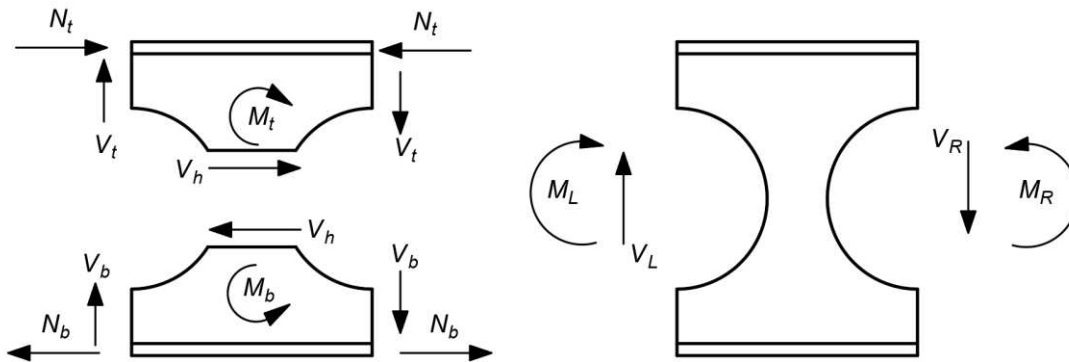
Keywords: Cellular beams; Elastic and inelastic buckling; Strong-axis bending; FEA; Parametric studies; Automated analyses; Python; Mass data

31 **1. Introduction**

32 *1.1 Background*

33 The use of steel beams is an attractive option within the steel construction industry due to its flexibility in
34 terms of strength, size, and weight. The most notable benefits of perforated beams are the inclusion of
35 services, thereby reducing the building's height, the need for internal columns, construction time and costs.
36 The increased depth of cellular beams offers greater bending resistance in the strong-axis which provides
37 an increased moment of inertia when compared to similar weight sections.

38
39 Perforated beams with circular web openings referred to as cellular beams have been found to have
40 additional merits relating to its flexibility and design when compared to other beams with varying opening
41 shapes. The presence of web openings, however, presents several intricate behavioural patterns due to the
42 combined shear and bending stresses concentrated at the openings. According to Ward (1990) the load-
43 carrying capacity of a cellular beam is significantly affected by the response of the web-post and the tee-
44 sections to local bending and vertical shear across the web opening. Consequently, over the years,
45 researchers have studied the stress distribution pattern and failure modes of these beams based on elastic
46 and inelastic behavioural patterns. Figure 1 displays a cellular perforated section in static equilibrium.



47
48 Figure 1: Forces in static equilibrium at the opening and the web-post

49 The aim of the current study is to highlight the effects of certain key parameters (e.g., material
50 nonlinearities, manufacture-introduced residual stresses, web opening diameters, web-post widths, heights
51 of web, widths of flange, flange thicknesses, web thicknesses, and lengths of beams) on the global structural
52 behaviour and ultimate load capacity through developing mass data. The global response was considered
53 as a combined interaction of the global lateral buckling mode and localised deformations at the openings.
54 The interaction of buckling modes in I-section beams (perforated and non-perforated) has been a subject of
55 extensive experimental and numerical investigations. For example, Bradford (1992, 1998) thoroughly
56 examined the lateral-distortional buckling of I-sections, Zirakian and Showtaki (2006) was one of the first
57 to study the distortional buckling of castellated beams, also Zirakian (2008) studied the elastic distortional
58 buckling of doubly symmetric I-shaped flexural members with slender webs, and Ellobody (2011, 2012,
59 2017) comprehensively investigated the interaction of buckling modes in castellated steel beams conducting
60 nonlinear analyses under combined buckling modes as well as studying the interaction of buckling modes
61 in steel plate girders. Ellobody (2012) concluded that the influence of the interactions of lateral-torsional
62 and web distortional buckling of cellular beams on the strength and inelastic behaviour is yet to be

63 understood. As such, this research sought to avoid the analysis of many complex localised failures
64 associated with cellular beams by utilising a FE collapse analysis to compute the global buckling capacity
65 as a Load Proportionality Factor (LPF) of the entire beam. Even though many researchers since 1957 (e.g.,
66 Altfillisch et al., 1957, Kolosowski J, 1964, etc.) investigated perforated beams; until the past decade where
67 scientists have studied various localised failures such as buckling (e.g., Ellobody, 2011) and vertical shear,
68 aka Vierendeel (e.g., Tsavdaridis and D’Mello, 2012; Tsavdaridis and Galiatsatos, 2015), very little has
69 been done with regards to the global response of such members.

70
71 With the power of today’s FE tools and CPU, this study provides an opportunity to fill this gap in the
72 literature, as extensive FE parametric analyses on the structural stability of thin-walled cellular beams can
73 attempt to clarify the influence of each parameter to the perforated beams’ complex structural behaviours.

74 *1.2 Failure Modes*

75 Past numerical and experimental studies on perforated beams have shown that the failure modes are
76 dependent on the slenderness of the section, the geometry of the web opening (i.e., diameter and web-post)
77 and the type of load application (Chung et al., 2003). The bending and shear stresses concentrate in the
78 vicinity of the openings and trigger several types of failure modes including web-post buckling, lateral-
79 torsional buckling (LTB) with web-distortion, Vierendeel mechanism and the rupture of the welded joints.

80
81 The excessive plastification of plastic hinges, or Vierendeel mechanism, commonly occurs in beams with
82 short spans, wide web-post, wide flange, and shallow tee-sections. This type of failure was firstly reported
83 by Alfillisch et al. in 1957 and later by Kolosowski, 1964, while it was comprehensively studied by Kerdal
84 and Nethercot (1984) to develop an in-depth understanding of the effects of the opening geometry. The past
85 decade, Tsavdaridis et al. presented a series of extensive research studies investigating the mobility and
86 position of plastic hinges when different shape and size of web openings are used and relate them with the
87 shear-moment interaction at the centreline of the particular opening. Experimental (Tsavdaridis 2010;
88 Tsavdaridis and D’Mello 2012) and FE (Tsavdaridis and D’Mello, 2009; Tsavdaridis and D’Mello, 2011)
89 studies have been conducted. Moreover, Kingman et al. (2015) proposed optimised architectures for web
90 openings to better control the position of the plastic hinges, increasing the capacity of the section.
91 Tsavdaridis and Galiatsatos (2015) have also studied the position of the plastic hinges and capacity gains
92 by the introduction web-welded stiffeners. Yu et al. (2010) and Tsavdaridis et al. (2013) also studied the
93 vertical shear capacity of such perforated sections when infilled by concrete. Later, Maraveas et al. (2017)
94 has examined the performance of such beams under fire conditions too. Overall, it was concluded that the
95 position of the plastic hinges drastically influences the beam’s load-carrying capacity.

96
97 This study seeks to activate a lateral global buckling failure combined with a localised web-post
98 deformation by alternating various magnitude of geometrical imperfections to the first global and local
99 buckling modes. Therefore, the collapse failure (e.g., at maximum LPF) is in the form of a lateral
100 distortional buckling (LDB) which consists of a combined effect of lateral movement, unequal twisting of
101 the flange and localised web distortion of the cross-section.

102
103
104
105

106 *1.3 Design Guidelines*

107 Akrami and Erfani (2016) compared the most prevalent design guidelines and concluded that the methods
108 proposed by Chung et al. (2003) and Tsavdaridis and D’Mello (2012) were the least restrictive as compared
109 to the other design methods (i.e., ASCE 23-97; SCI-P100; SCI-P355) and produced the lowest errors.
110 However, even though design methods have been presented, there are still several uncertainties that result
111 in conservative and complicated design approaches. Therefore, the complexity of perforated beams and the
112 numerous parameters which affect the performance indicate the need for further research - most importantly
113 in the global response. In the design guidelines, some of the failure modes or a combination of failure modes
114 and parameters are excluded, thus they are restrictive approaches.

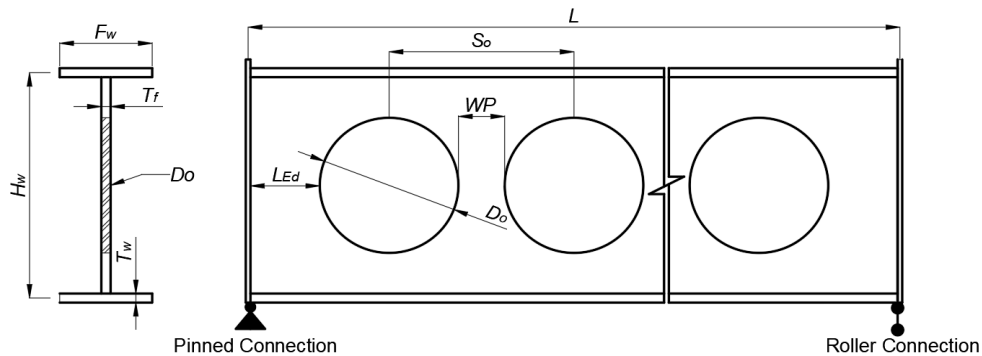
115
116 **2. Parametric Matrix and Finite Element Modelling**

117 The variables required for the elastic analysis is only based on the linear elastic stiffness, boundary
118 conditions, and geometry. The parametric study required the creation of 405 ABAQUS CAE base models.
119 The non-scripted parameters were the spacing of web opening (3 values), the diameter of web opening (3
120 values), the height of section (3 values), the width of the flange (3 values) and length of member (5 values).

121
122 The total number of combinations generated with Python for each analysis type is as follow:

- 123 • Elastic analysis = 3^6 (x 5 lengths) = 3,645 FE simulations
- 124 • Nonlinear analysis = 3^9 (x 5 lengths) = 98,415 FE simulations

125
126 The critical geometrical parameters are provided in Figure 2.



127

128 **Figure 2:** Important dimensional parameters of cellular beams

129 *2.1 Geometric Parameters of Cross-Section*

130 The lengths of beams selected for this study were 4m, 5m, 6m, 7m, and 8m. It was decided not to examine
131 longer beams as the effect of the web opening is less critical to local failure mechanisms. According to
132 Chung et al. (2001) and Tsavdaridis (2010) the longer the beam is, the less is the effect of the web opening
133 position – a critical parameter for this study. When perforated sections with large web openings are
134 considered, the combination of the beam span and the web opening position could yield completely
135 different results. In particular, for long span beams (>7m) and web openings located close to the mid-span;
136 the global bending moment at the perforated section increases quickly while the shear force decreases
137 steadily. Therefore, the beams tend to fail in flexure due to a reduced moment capacity of the perforated

138 section. However, for short span beams a reduced load carrying capacity is obtained when the web openings
 139 are located either close to the supports or close to the mid-span. Obviously, the reduction of the shear
 140 capacity for large web openings close to the support is more severe. For conservative reasons, it is decided
 141 to use spans up to 8m for this research programme as the fluctuation of the results using large web openings
 142 leads to important conclusions. The fillet radius has been neglected in high impact research relating to
 143 cellular beams (Ellobody E, 2012; Tsavdaridis and D'Mello, 2011, 2012; Wang, Ma and Wang, 2014) and
 144 design guidelines (AISC, 2017), therefore, the influence is considered insignificant to alter the beam's
 145 global response, and it is not considered as a parameter variable for this study. This assumption is also in
 146 line with Sonck (2014) and Taras (2010) who have reported that this simplification by ignoring the fillet
 147 radius effects is small on the buckling curve parameters. This approach is also conservative and covers the
 148 case where fabricated sections are considered. The cross-section properties of the beams are summarised in
 149 Table 1.

151 **Table 1:** Cross-sectional description of beams

Description	Variable (1) (mm)	Variable (2) (mm)	Variable (3) (mm)
Web height (H_w)	700	560	420
Web thickness (T_w)	15	12	9
Flange width (F_w)	270	216	162
Flange thickness (T_f)	25	20	15

152
 153 **2.2 Web Opening Limits**

154 The web opening diameter and spacing were limited to the recommended range in accordance with SCI-
 155 P100 ($H_w/D_o=1.25$ to 1.7 and $S_o/D_o= 1.1$ to 1.49). Table 2 provides the geometrical parameters for the
 156 perforation. It is worth noting that the location of the first web opening in the parametric study was placed
 157 at the centre of the beam while the subsequent adjacent openings were offset from the central opening until
 158 no more web opening can fit in the beam's length. This approach resulted in 135 different distances from
 159 the end perforation to the support (centreline of end-plate) which was also considered as an independent
 160 variable (L_{Ed}).

161 **Table 2:** Spacing between web openings with respect to the opening diameter

(H_w) (mm)	D_o (mm) ($H_w/1.25, H_w/1.5$ & $H_w/1.7$)	(S_o) (mm)			WP (mm)		
		$1.1D_o$	$1.29D_o$	$1.49D_o$	$D_o/10$	$D_o/3.45$	$D_o/2.04$
700	560	616	722	834	56	162	274
	467	514	602	696	48	135	229
	412	453	531	613	41	119	202
560	448	493	578	668	45	130	220
	373	410	481	556	37	108	183
	329	362	424	490	33	95	161
420	336	370	433	501	37	97	165
	280	308	361	417	28	81	137
	247	272	319	368	25	72	121

162 **2.3 Material Properties**

163 The material behaviours used are elastic and elasto-plastic with isotropic strain hardening, which considered
 164 a tangential modulus of (E_t) 1000MPa, a Modulus of Elasticity of (E) 200GPa, and a Poisson's ratio of 0.3.
 165 The Tangent modulus assumption utilised after a detailed study of the test data taken from Redwood and
 166 McCutcheon (1968). The three combinations selected are presented in Table 3.

167
 168 **Table 3:** Material nonlinearities for the three selected strength class for steel

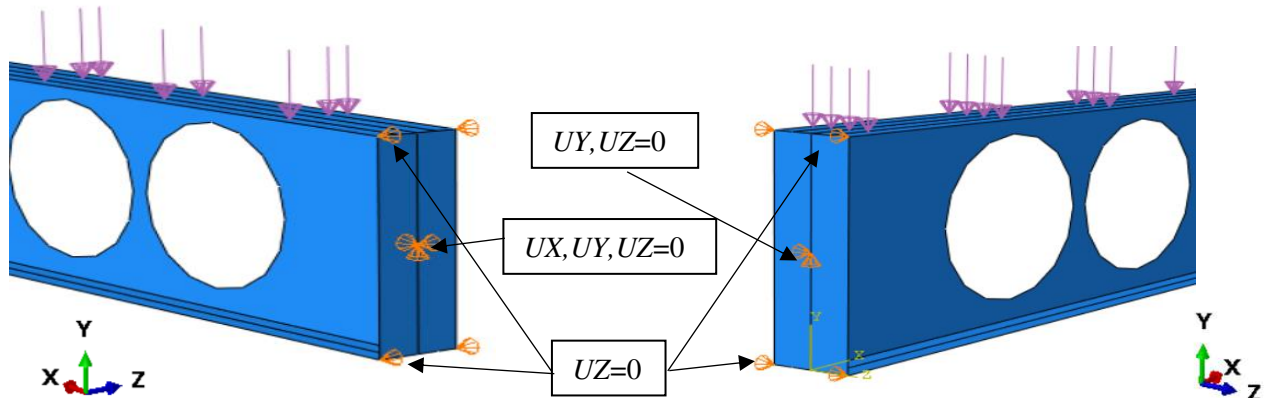
Yield stress (MPa) f_y	Ultimate stress (MPa) f_u	Initial Strain (ϵ_y) f_y/E	Final Strain (ϵ_t) $\epsilon_y + (f_u - f_y)/E_t$
235	360	0.001175	0.156775
355	510	0.001775	0.126175
440	550	0.0022	0.1122

169
 170 **2.4 Finite Element Properties**

171 The geometry of the models was prepared using planar shell models having homogenous material
 172 properties. The finite element mesh uses the quad-dominated, type S8R (e.g., stress-displacement shell with
 173 eight nodes) doubly curved thick shell elements using reduced integration element which has six degrees
 174 of freedom per node. Sonck (2014) reported this is ideal for modelling cellular beams as hour-glassing
 175 would occur for the reduced order shell elements (e.g., S4R and S4R5). The consideration for the mesh was
 176 taken from Hesham Martini (2011) and Sweedan, (2011) where 12 elements are across the flange width
 177 and size for the web region was reduced by 20% (e.g., $F_w/12*1.2$). Support endplate uses 8 elements as this
 178 is unimportant. This arrangement has been observed, to accurately predict the global response of cellular
 179 beams tested in laboratory by Surtees and Liu (1995) and Tsavdaridis and D’Mello (2011) as detailed in
 180 section 3.0 and was effectively implemented for computational application in Abambres et al. (2018).

181 **2.5 Boundary and Loading Conditions**

182 The models considered a simple supported connection where one end was pinned and the other was a roller.
 183 This allowed an in-plane rotation but not a translation at one end while the other one permits the translation
 184 of the beam beyond the in-plane rotation point. Twisting rotations at the ends were prevented by restraining
 185 both the top and bottom flange tips against out-of-plane displacements. (Ellobody, 2012) A uniformly
 186 distributed unit load was applied to the top flange which gives the critical buckling load and the collapse
 187 load LPF as a multiplier of 1.0.



188
 189 **Figure 3:** Boundary conditions in the finite element model

190

191 *2.6 Initial Geometric Imperfection*

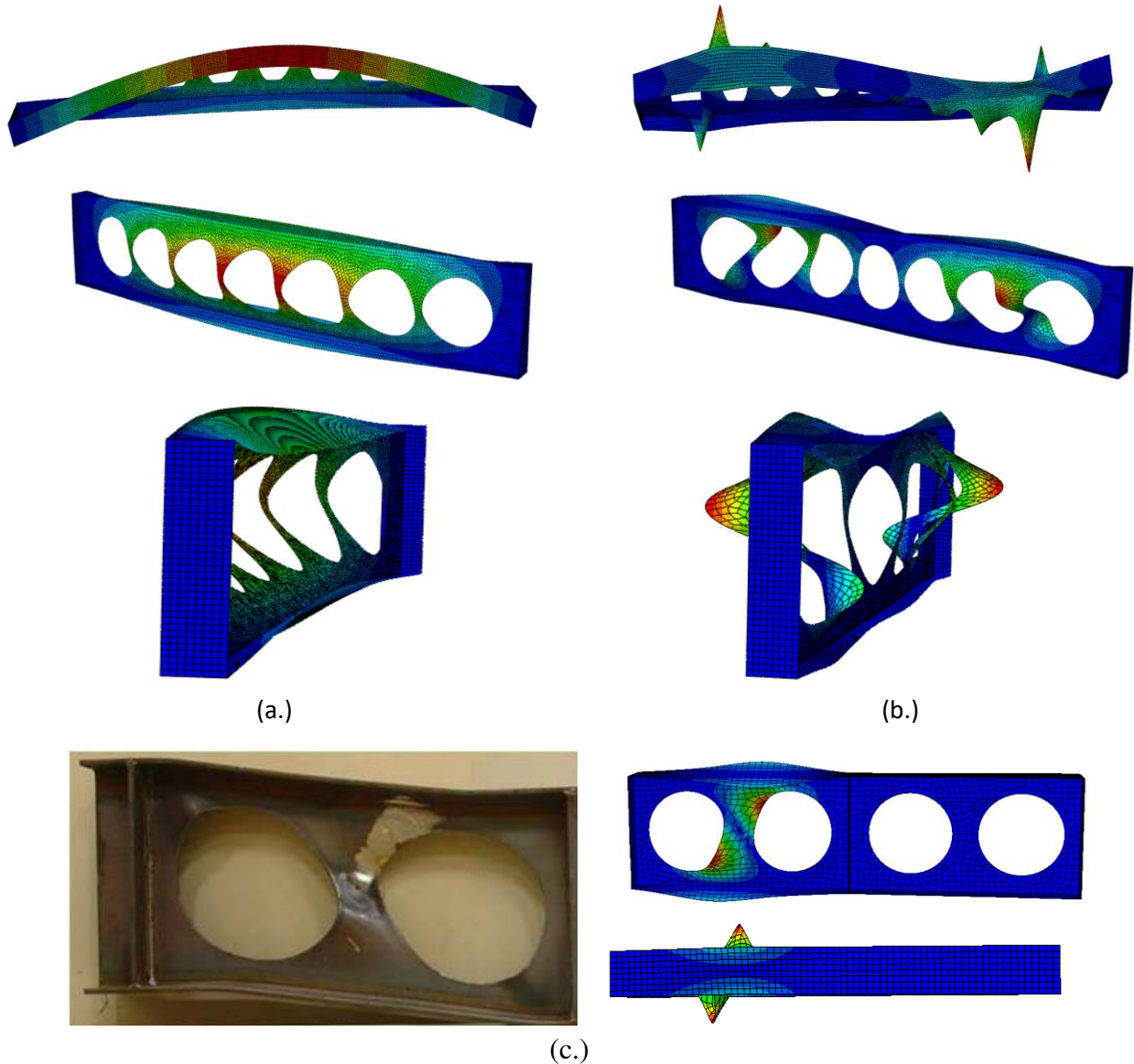
192 Imperfections allow the initiation of buckling failure; however, this imperfection must be of small
193 magnitude in order to avoid disruption of the beam's main responses. The global imperfection was applied
194 to the first Eigen buckling mode and the local imperfection to the second or third Eigen buckling mode. As
195 the beam length increases, the first two modes produced global perturbation shapes. The global
196 imperfections (δ_g) scale was taken as $L/2500$, $L/2000$, and $L/1500$.

197

198

199

200



201

202

203

204 **Figure 4:** Perturbed geometry: (a) the global, (b) local initial geometrical imperfection shapes (local
205 buckling near the supports), (c) Image of local imperfection (Tsavdaridis and D'Mello, 2011)

206

207

The local imperfection was based on Dawson and Walker (1972) method which is a function of the cross-section of the beam and the yield strength of steel. The following equations were utilised to calculate the

208 local imperfection for the web region as provided in Table 4. This imperfection shape only captured the
 209 web distortion buckling mode. The calculations incorporated a yield strength (f_y) of 355MPa.

$$210 \quad \delta_{LI} = \frac{\gamma T_w f_y}{\sigma_{cr,l}} = \frac{\gamma f_y (H_w)^2}{21.6 E T_w} \quad (\text{eq1})$$

$$211 \quad \sigma_{cr,l} = \frac{23.9 \pi^2 E}{12 (1 - 0.3^2)} \left(\frac{T_w}{H_w} \right)^2 = 21.6 E \left(\frac{T_w}{H_w} \right)^2 \quad (\text{eq2})$$

212 The third local geometrical imperfection was chosen based on the following parameters in order to
 213 considered a localised imperfection that is slightly higher than what is specified by Dawson and Walker
 214 (1972).

$$215 \quad \delta_{LI(3)} = \frac{\left(\frac{F_w}{z} \right)}{200} = \frac{C_{flange}}{200} \quad (\text{eq3})$$

216

217 **Table 4:** Local web imperfection applied to the web buckling deformed mode

Formulae	$T_w = 15\text{mm}$ $H_w = 700\text{mm}$	$T_w = 12\text{mm}$ $H_w = 560\text{mm}$	$T_w = 9\text{mm}$ $H_w = 420\text{mm}$
$\delta_{LI(1)} = \frac{0.1 T_w f_y}{\sigma_{cr,l}}$	0.268441358	0.214753086	0.161064815
$\delta_{LI(2)} = \frac{0.2 T_w f_y}{\sigma_{cr,l}}$	0.536882716	0.429506173	0.32212963
$\delta_{LI(3)} = \frac{C_{flange}}{200}$	0.675	0.54	0.405

218

219

220 2.7 Residual Stresses

221 During the cutting and welding process, the use of heat can lead to uneven cooling along with the member
 222 resulting in variable yield stress patterns and further differential plastic deformations (Sonck, 2014). The
 223 process of welding can cause a thermal contraction as the beam cools which may result in residual tension
 224 in the areas of the weld; as this takes longer to cool and compression in sections further away from the
 225 welded region may occur (Sonck, 2014; Schwail, 2013). The residual stress pattern shown in Figure 5 was
 226 based on the findings reported by Snock (2014) for cellular beams where the web of the beam is subjected
 227 to tensile stresses. The flange has both tension and compression stresses similar to those presented by
 228 Tebedge (1973).

229

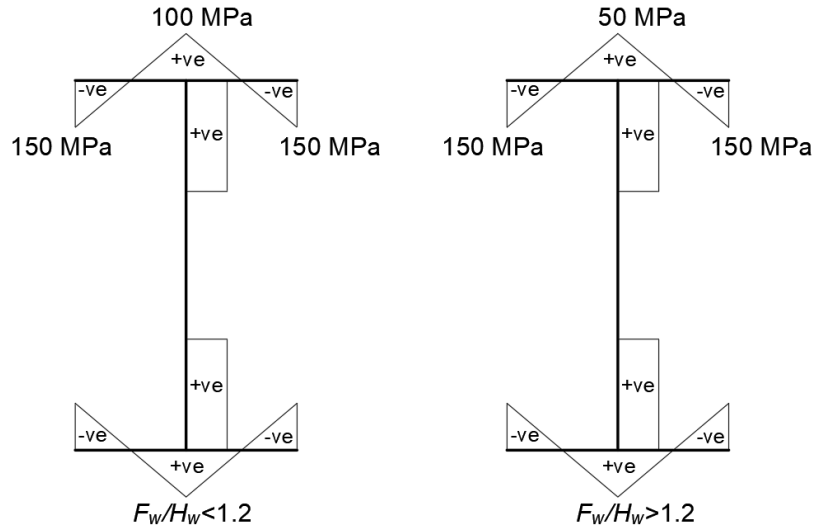


Figure 5: Residual stress pattern employed

230
231

232

233 *2.8 Inelastic Analysis (Static Riks Method)*

234 The static Riks method has the ability to keep the beam in equilibrium at every load increment during
 235 unstable phases of the analysis. Therefore, the analyses do not terminate at maximum LPF and then go into
 236 a snap-through response as the beam's geometry changes which yields a lower LPF in the parametric study.
 237 Due to no stopping criterion at maximum LPF in ABAQUS, the arc-length increment was specified for
 238 each of the 405 models in the Python script to allow for the termination of the analyses before the onset of
 239 the snap-through response. This was done by monitoring $405 \times 3 = (1215)$ simulations.

240

241 *2.9 Application of Geometric Imperfections and Residual Stresses*

242 The initial geometric imperforation was introduced by using the perturbation in the geometry generated
 243 from the elastic buckling analysis by applying a scale factor (local and global imperfection). Following the
 244 introduction of the initial stresses, a general static step was required to allow the beam to regain its
 245 equilibrium before the load step. The static Riks step was then introduced to continue the analysis into the
 246 nonlinear response.

247

248 *2.10 LPF Output*

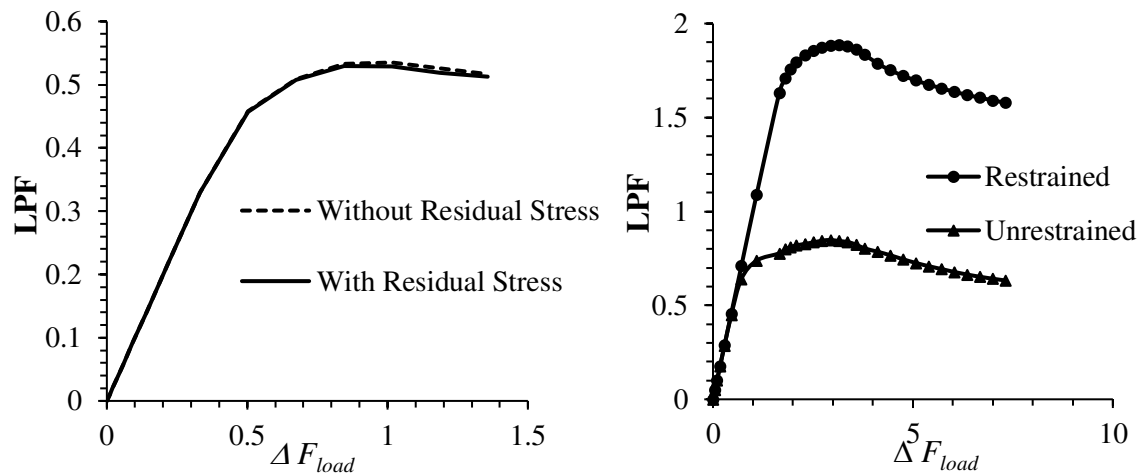
249 To establish LPF as a variable, it was required to request all displacement history output for a particular
 250 node in the model. The location of the node selected in the model is insignificant as LPF output variable is
 251 for the entire model response, therefore, in the Python script, a 'gather' and 'output' command was used to
 252 extract the LPF for a specific increment at maximum LPF.

253

254 **3. FE Validation Study**

255 The FE models were validated employing two experimental models found in the literature (Tsavdaridis and
 256 D'Mello, 2011; Surtees and Liu, 1995), including the response of a short beam to local web-post buckling
 257 failure and a longer beam to capture the global response with the combination of web distortional buckling.

258 Both validations were considered satisfactory with results within 3% of the load capacity recorded by the
 259 experiment. In Figure 5.a, the collapse load (P_{CL}) computed was $0.52 * 572,009\text{N}$ (e.g., Eigen-mode 1,
 260 elastic buckle load $572,009\text{N}$) = 297kN and the experimental results is 288.7kN in Tsavdaridis and D’Mello
 261 (2011) for a 1.7m length beam. For a longer restrained/braced beam, the experiment P_{CL} by Surtees and Liu
 262 (1995) is 188.5kN and in Figure 5.b the LPF is 1.87 (e.g., $1.87 * 100,000\text{N}$ is 187kN). Therefore, it is safe
 263 to conclude that the Methodology adopted provides accurate results. For more information, please refer to
 264 Tsavdaridis and D’Mello (2011).
 265



266 **Figure 6:** Collapse loading (LPF) of the beam. (a) Tsavdaridis and D’Mello, 2011 and (b) Surtees and
 267 Liu, 1995
 268

269 **4. Results and Discussion**

270 *4.1 FEA and SCI P355 Results*

271 Figure 7 demonstrates that the SCI P355 analytical method produced conservative load-carrying capacities
 272 as compared to that of the FEA models. It is also noticeable that the differences between the two
 273 computational methods do not produce a similar percentage of variance (pattern) in the load-carrying
 274 capacity for the 8 selected beams, while the inelastic results are compared very well with the SCI P355
 275 calculation. For example, beam 'A11' and beam 'A25' has a percentage variance of 6% and 45%,
 276 respectively. Beam 'A11' shows that the SCI P355 overestimated the capacity because the end distance from
 277 the last opening to the edge of the beam was not incorporated in the SCI design calculations. On the
 278 contrary, the narrow end distance which governed the analysis in FEA. In another case, beam 'A25', where
 279 the end distance is larger, SCI P355 method resulted in a very conservative low load as compared to the
 280 FEA, while the web-post buckling would always govern the design using the SCI P355 for beams with
 281 slender web-posts (i.e., closely spaced web openings). Therefore, for slender WP, web buckling will always
 282 govern the design in SCI P355. As for the FEAs, the end distance parameter governs the design for widely
 283 spaced web openings. It is worth to note that SCI P355 does not consider L_{Ed} but recommends $\geq 0.5D_o$.
 284

285 It should be noted, that the simple strut approach model adopted in SCI P355 underestimates the true
 286 capacity of the web-post for slender web-post (e.g., $D_o/3.45$ to $D_o/10$) and a revision is necessary to improve
 287 the accuracy. However, SCI P355 provides accurate results for widely spaced openings (e.g., web-post $>$
 288 $D_o/3.45$) as the Vierendeel bending approach adopted is suitable to estimate the shear across the opening.
 289

290
291
292

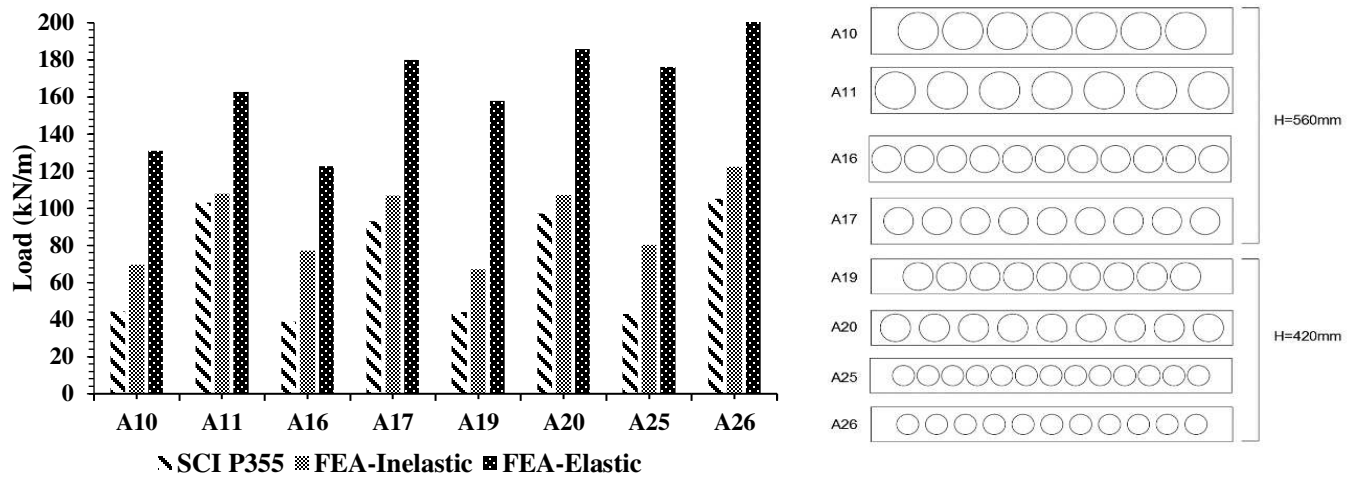
Table 5 - Independent variable combination for SCI P355 design comparison

Ref #	L (mm)	T_w (mm)	T_f (mm)	F_w (mm)	H_w (mm)	D_o (mm)	WP (mm)
A10	4000	9	15	162	560	448	45 *
A11					560	448	130 **
A16					560	329	33 *
A17					560	329	95 **
A19					420	336	34 *
A20					420	336	97 **
A25					420	247	25 *
A26					420	247	72 **

293
294
295
296

* = $0.1d_o$
** = $0.3d_o$

297 Figure 7 includes the elastic buckling load (γ_{cr}) is considerably high which concludes that the γ_{cr} should be
298 used with caution as imperfection and initial stresses are always present. The γ_{cr} seems to be in the region
299 of approximately 45% more than the nonlinear buckling load.
300



301
302

Figure 7: SCI P355, inelastic and elastic buckling load comparison, $L = 4m$

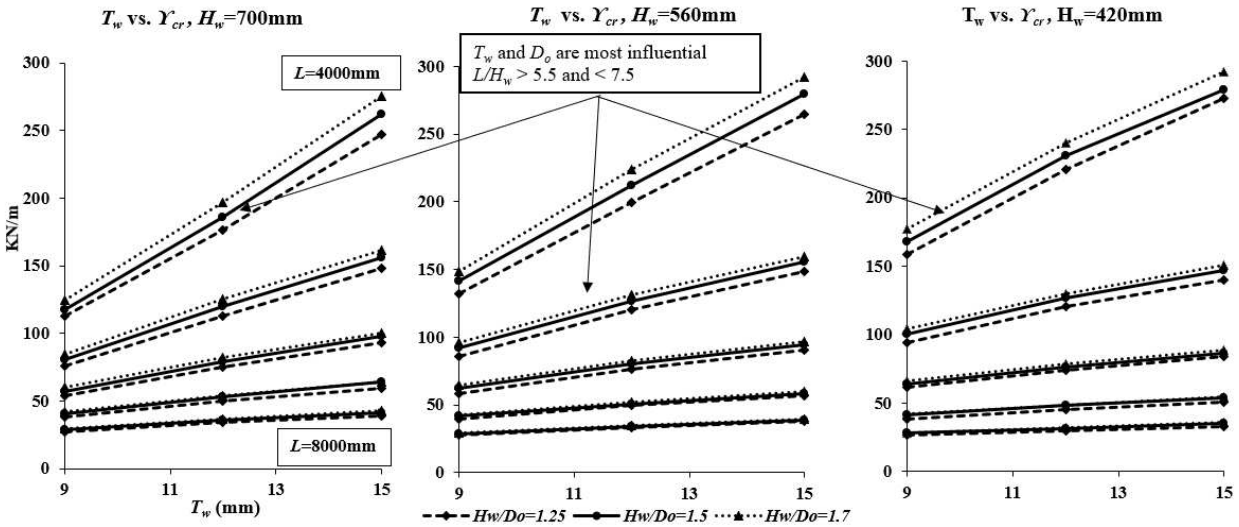
303
304

4.2 Results of Elastic Analyses

305 This section contains an analysis of the relationships of the effects of the independent variables on the
306 dependent out variable (γ_{cr}). The graphs were analysed with respect to the T_w and D_o as a function of the
307 H_w . Figure 8 demonstrates the effects of the length (L) and H_w with the constant parameters $D_o/WP = 10$,
308 $F_w = 162mm$ and $T_f = 15mm$.

309 In Figure 8, the H_w is an insignificant parameter since the first buckling mode corresponded to a lateral
 310 buckling and therefore the F_w is a critical parameter to restraint the lateral movement. The effects of D_o
 311 (e.g., $H_w/D_o = 1.25$ to 1.7) and the effects of T_w (e.g., 9mm to 15mm) are as follow:

- 312 - $5.5 \geq L/H_w \leq 7.5$, D_o effects are approximately 10.5% and T_w increases the Y_{cr} by about 98%.
- 313 - $7.5 \geq L/H_w \leq 10.5$, D_o effects are approximately 7.5% and T_w increases the Y_{cr} by about 62%.
- 314 - $10.5 \geq L/H_w \leq 13.5$, D_o effects are approximately 7.0% and T_w increases the Y_{cr} by about 45%.
- 315 - $13.5 \geq L/H_w \leq 19$, D_o effects are approximately 6.5% and T_w increases the Y_{cr} by about 30%.

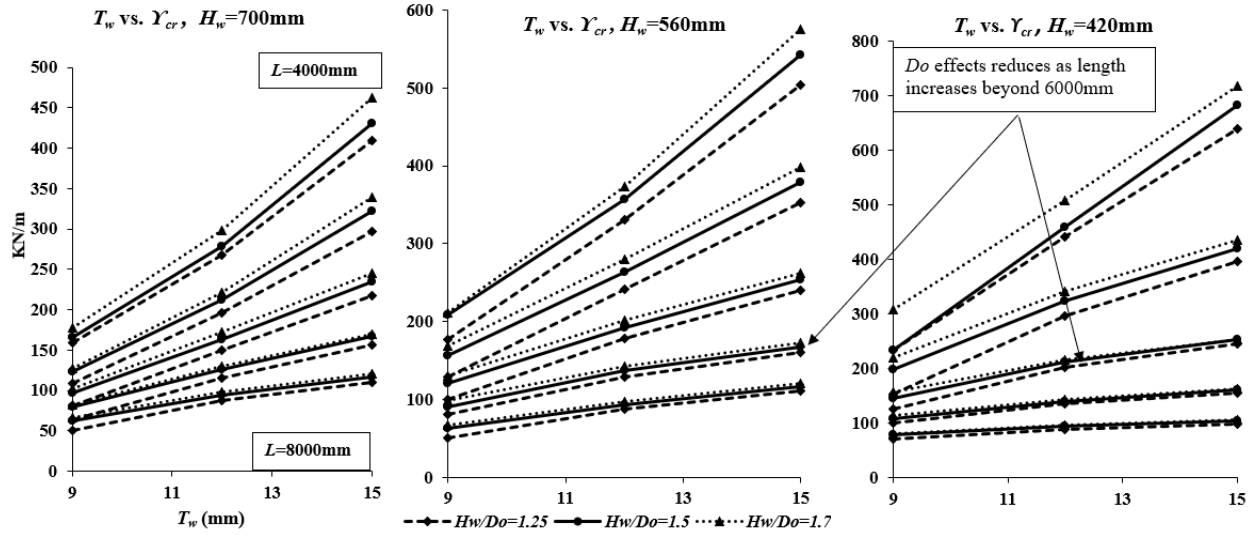


316
 317
 318 **Figure 8:** Effects of H_w on the elastic load (Y_{cr}) with respect to varying T_w and L : 4m to 8m

319 In Figure 9, the F_w was increased from 162mm to 270mm. The change in F_w positively impacted the Y_{cr} as
 320 lateral movement is restricted and the gradient of the plot increased greatly with the change in T_w (e.g.,
 321 15mm to 25mm). The following was concluded:

- 322 - $5.5 \geq L/H_w \leq 7.5$, D_o effects are approximately 14% and T_w increases the Y_{cr} by about 150%.
- 323 - $7.5 \geq L/H_w \leq 10.5$, D_o effects are approximately 11.5% and T_w increases the Y_{cr} by about 140%.
- 324 - $10.5 \geq L/H_w \leq 13.5$, D_o effects are approximately 8.5% and T_w increases the Y_{cr} by about 110%.
- 325 - $13.5 \geq L/H_w \leq 19$, D_o effects are approximately 5.5% and T_w increases the Y_{cr} by about 45%.

326 Comparing Figures 8 and 9 by increasing the F_w for critical members (e.g., $5.5 \geq L/H_w \leq 7.5$) the load
 327 increased is in the region of 85% and for slightly less slender members (e.g., $7.5 \geq L/H_w \leq 10.5$) the F_w
 328 effects has increases to 135%.



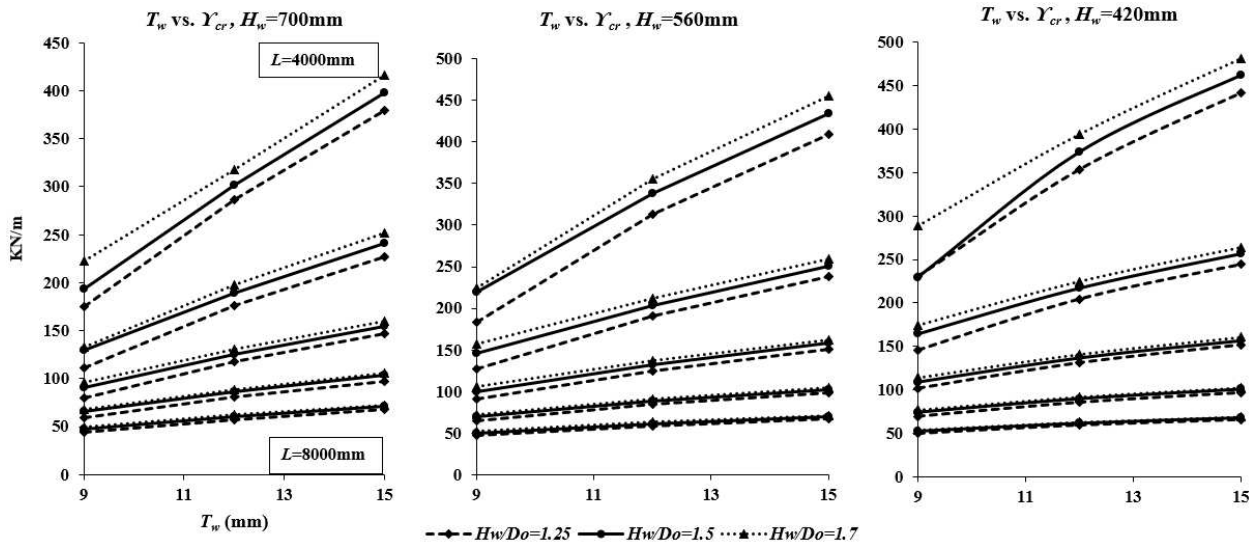
329
330

Figure 9: Effects of increasing the F_w from 162mm to 270mm from Figure 7

331 Figure 10 compared the effects of varying T_f from 15mm to 25mm. The following was concluded:

- 332 - $5.5 \geq L/H_w \leq 7.5$, D_o effects are approximately 10.5% and T_w increases the Y_{cr} by about 93%.
- 333 - $7.5 \geq L/H_w \leq 10.5$, D_o effects are approximately 7.0% and T_w increases the Y_{cr} by about 72%.
- 334 - $10.5 \geq L/H_w \leq 13.5$, D_o effects are approximately 5.1% and T_w increases the Y_{cr} by about 49%.
- 335 - $13.5 \geq L/H_w \leq 19$, D_o effects are approximately 4.0% and T_w increases the Y_{cr} by about 35%.

336 Comparing Figures 8 and 10 by increasing the T_f for critical members (e.g., $5.5 \geq L/H_w \leq 7.5$) the load
337 increased is in the region of 53% and for slightly more flexible slender members (e.g., $7.5 \geq L/H_w \leq 10.5$)
338 the T_f effects has increases to 62.3%.



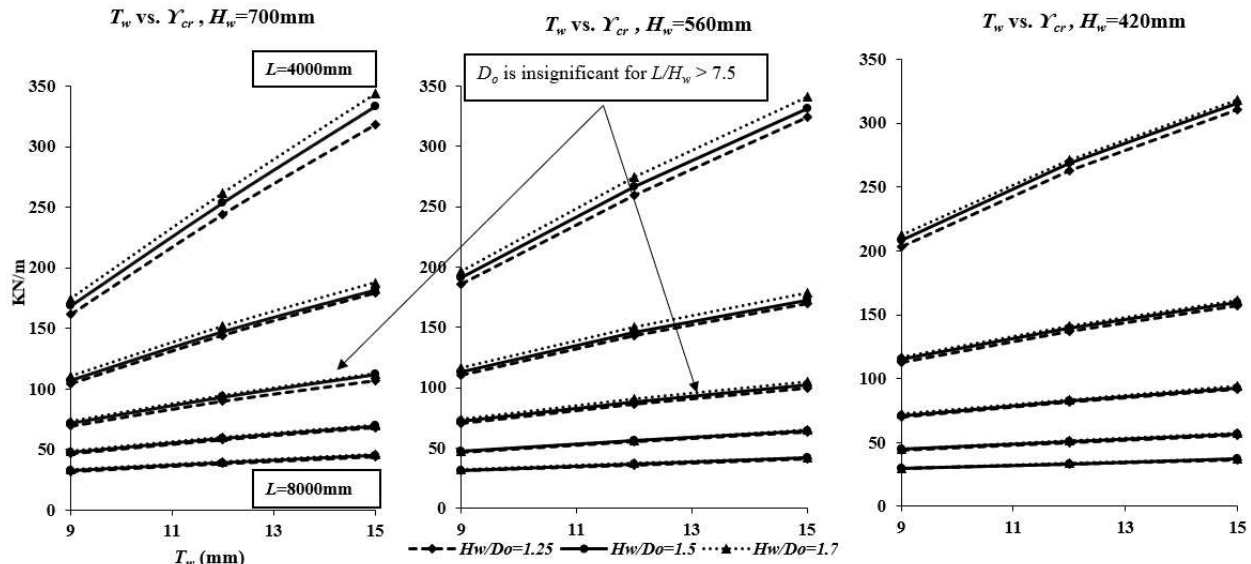
339
340

Figure 10: Effects of varying the T_f : 15mm to 25mm from Figure 7

341 Figure 11 considers the effects of the web-post width from $D_o/10$ to $D_o/2.04$. The change in the D_o parameter
342 had little effect on the Y_{cr} for wider WP. The results are outlined as follow:

- 343 - $5.5 \geq L/H_w \leq 7.5$, D_o effects are approximately 6% and T_w increases the Y_{cr} by about 78%.
- 344 - $7.5 \geq L/H_w \leq 10.5$, D_o effects are approximately 2.75% and T_w increases the Y_{cr} by about 37.5%.

345 Figure 11 shows that for $L/H_w > 10.5$, the other parameters (e.g., D_o , H_w , T_w) had a minimum effect on the
 346 γ_{cr} . Based on Figures 8 and 11, increasing the $WP = H_w/2.04$ for critical members (e.g., $5.5 \geq L/H_w \leq 7.5$)
 347 the load increased is in the region of 20.5% and for slightly more flexible members $7.5 \geq L/H_w \leq 10.5$ the
 348 increase is 12.5% from Figure 8.



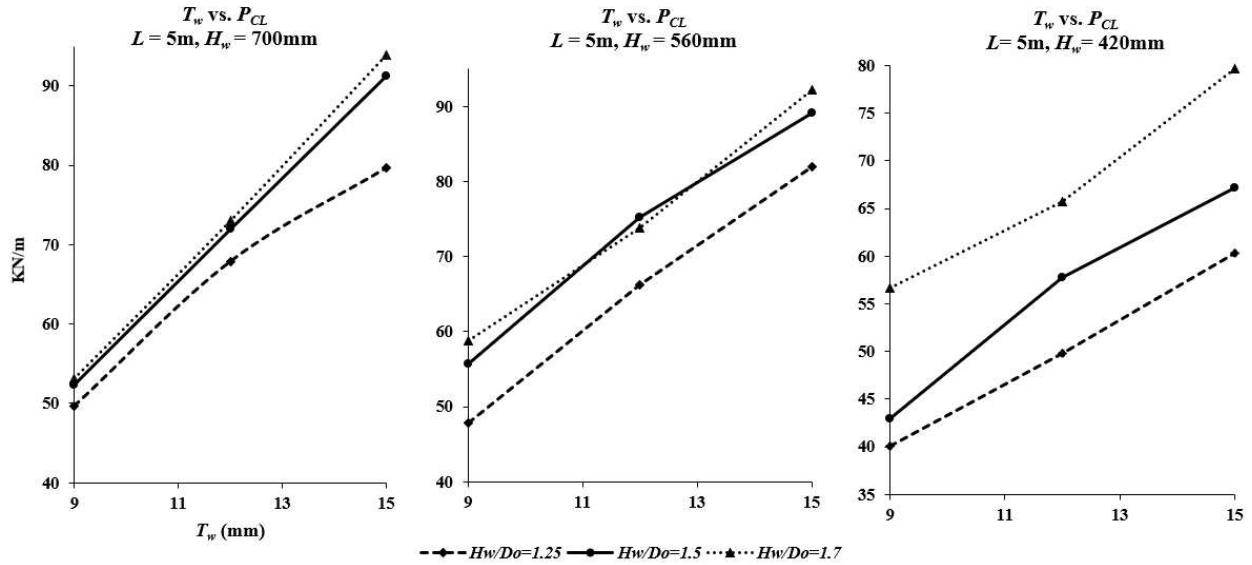
349
 350

Figure 11: Effects of varying Web-post width: $D_o/10$ to $D_o/2.4$ from Figure 7

351 **4.3 Results of Inelastic Analyses**

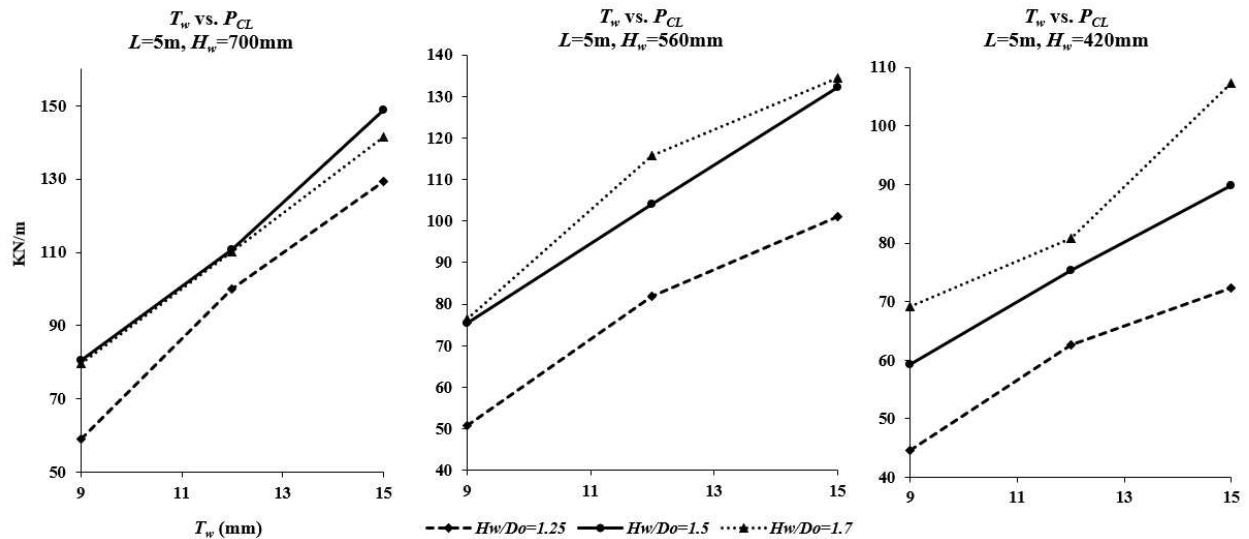
352 Inelastic results were analysed similar to Figures 8 to 11, however, the inelastic data were only analysed
 353 for $L=5m$ (e.g., $L/H_w = 7.15$ to 12) as it was observed for flexible members (e.g., $L/H_w > 12$) the effects of the
 354 other parameters become insignificantly. In addition, the effect of the length is already known from Chung
 355 et al. (2003) and Tsavdaridis (2010). The constant variables used for the inelastic analyses are F_y : 355MPa,
 356 T_f : 15mm, F_w : 162mm, δ_g : 2.1mm, δ_{LI} : 0.268441mm, D_o/WP : 10, ϵ_y : 0.001775 and ϵ_f : 0.126175.

357 In Figure 12, the three graphical responses demonstrate the effects of T_w is the most critical parameter as it
 358 controls the web behaviour even when the opening diameter varies. The change in T_w from 9mm to 15mm
 359 impacted the inelastic collapse load (P_{CL}) as L/H_w : 7.15, the load increased by 71.9%, L/H_w : 8.9 (60%) and
 360 L/H_w : 11.9 (56.5%). The average increase per 1mm change in T_w is approximately 10.5% in P_{CL} . The effects
 361 of D_o (e.g., H_w/D_o : 1.25 to 1.7) are in the region of 20% which is fairly significant when compared to Figure
 362 8.
 363



364
365 **Figure 12:** Effects of the H_w on the inelastic load (P_{CL}) with respect to varying T_w

366 Figure 13 utilised the parameters as Figure 12 however, in this case, the F_w was increased from 162mm to
367 270mm. The change in the F_w significantly increase the load capacity since first buckling mode experienced
368 a lateral buckling movement of the compression flange therefore with a wider F_w , the δ_g scale in Figure 4
369 has a lesser impact on the P_{CL} . As such, the effects of T_w for $L/H_w = 7.15$, load increased by 87.1%, $L/H_w =$
370 8.9 (76.1%) and $L/H_w = 11.9$ (51.5%). The average increase per 1.0 mm change in T_w is approximately 12%
371 in P_{CL} which is similar to Figure 12. The effects of D_o (e.g., H_w/D_o : 1.25 to 1.7) is in the region of 31.9% as
372 such the effects of the D_o increase with the changing in F_w .

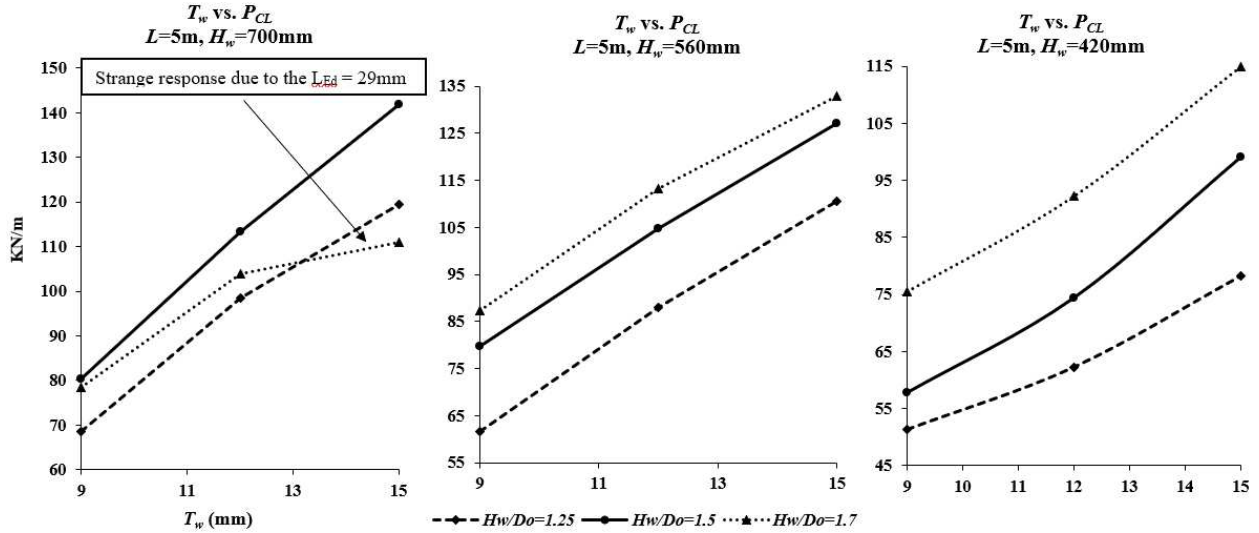


373
374 **Figure 13:** Effects of the F_w : increased from 162mm (as in Figure 12) to 270mm

375 Figure 14 considered the effects of T_f from 15mm to 25mm. The effects seem to have a similar response to
376 increasing the F_w (e.g., 162mm to 270mm). The change in T_w for $L/H_w = 7.15$, increased P_{CL} by 79.5%,
377 $L/H_w = 8.9$ (by 74.2%) and $L/H_w = 11.9$ (by 52.5%). The average increase per 1.0 mm change in T_w is

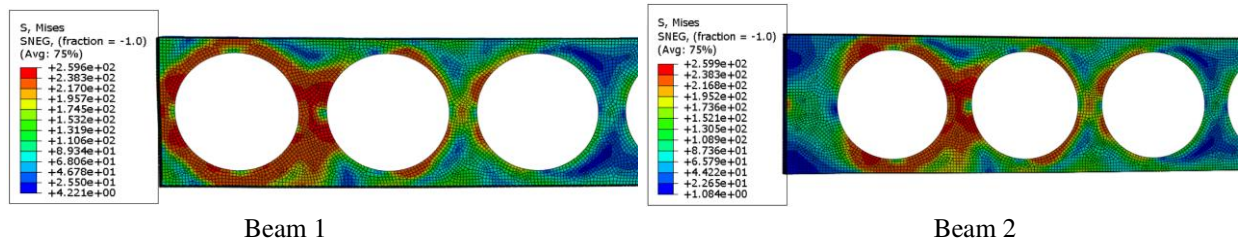
378 approximately 12% in P_{CL} which is similar to Figures 11 and 12. The effects of D_o (e.g., H_w/D_o : 1.25 to
 379 1.7) is in the region of 33.6% (similar to Figure 12).

380
 381 The first graph in Figure 14 ($H_w=700\text{mm}$) shows a strange response when $H_w/D_o=1.7$. This is because the
 382 end distance (L_{Ed}) was only 29mm. The L_{Ed} could not be analysed by these basic graphs as each beam had
 383 a different end distance resulted from the aforementioned design limitations.



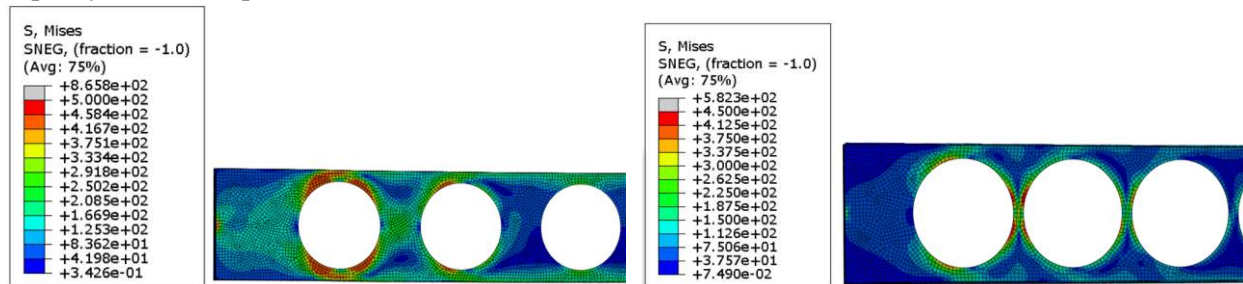
384
 385 **Figure 14:** Effects of the T_j : increased from 15mm (as in Figure 12) to 25mm

386 Figure 15 highlights the effects of the narrow L_{Ed} , which influence the load-carrying capacity as stresses
 387 are concentrated in the end region very early in the inelastic analysis.



388
 389 **Figure 15:** Comparison of stress concentration at maximum LPF for identical beams having varying
 390 end-distance (L_{Ed}) of 150mm at maximum LPF. (Collapse load: Beam 1 = 0.37MPa and Beam 2 =
 391 0.40MPa)
 392

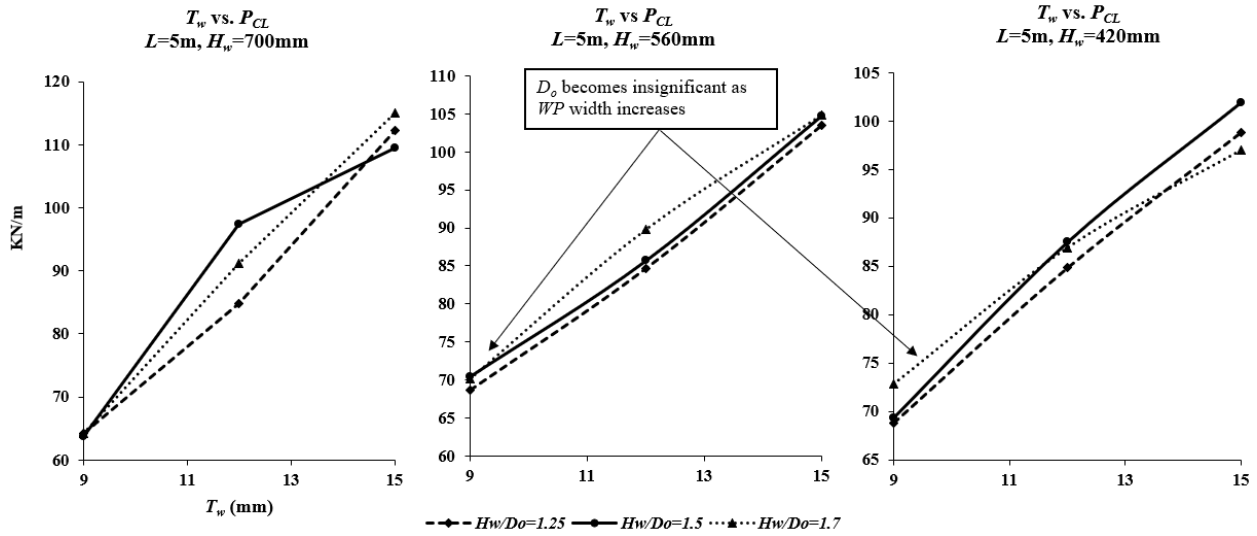
393 Figure 16 highlights the von-mises stresses concentration for varying the wed-post width (e.g., from $D_o/10$
 394 to $D_o/2.04$) for a similar span and section height. The end distance (L_{Ed}) does not influence the load carrying
 395 capacity in this comparison.



396

397 **Figure 16:** Comparison of stress concentration at maximum LPF for similar beams with varying web-post
 398 width. (e.g., $D_o/10$ to $D_o/2.04$)
 399

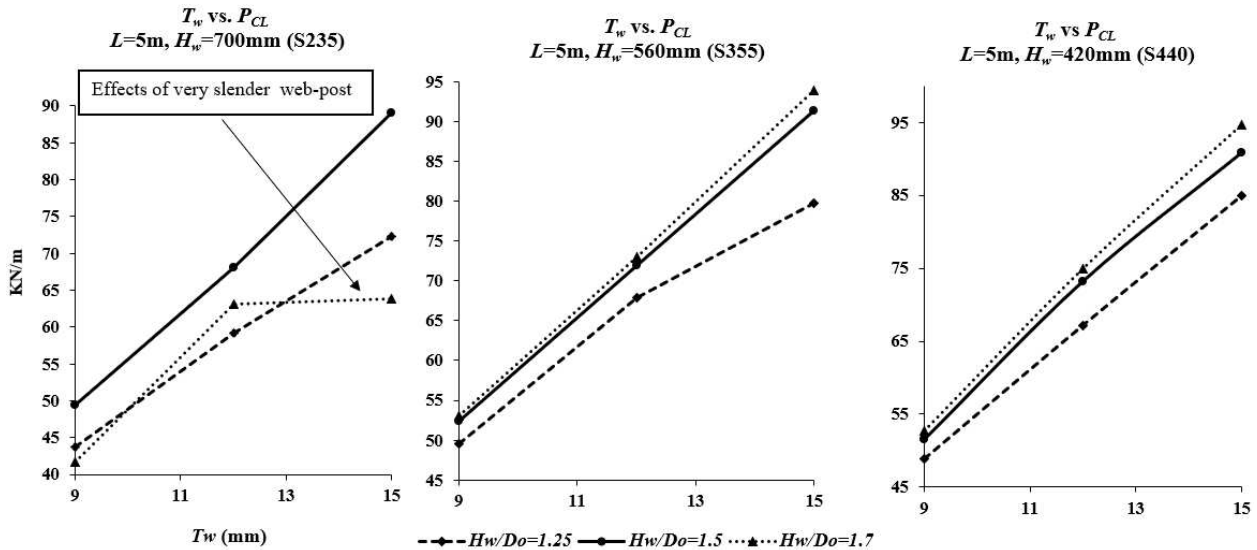
400 Figure 17 depicts the effects of the WP (e.g., $D_o/10$ to $D_o/2.04$). The change in T_w for $L/H_w = 7.15$, load
 401 increased by 77.3%, $L/H_w = 8.9$ (49.3%) and $L/H_w = 11.9$ (33.2%). The effects of increasing the WP to
 402 $D_o/2.04$ resulted in a P_{CL} increase of approximately 17.5% when compared to Figure 12.



403

404 **Figure 17:** Effects of the Web-post width from $D_o/10$ (as in Figure 12) to $D_o/2$

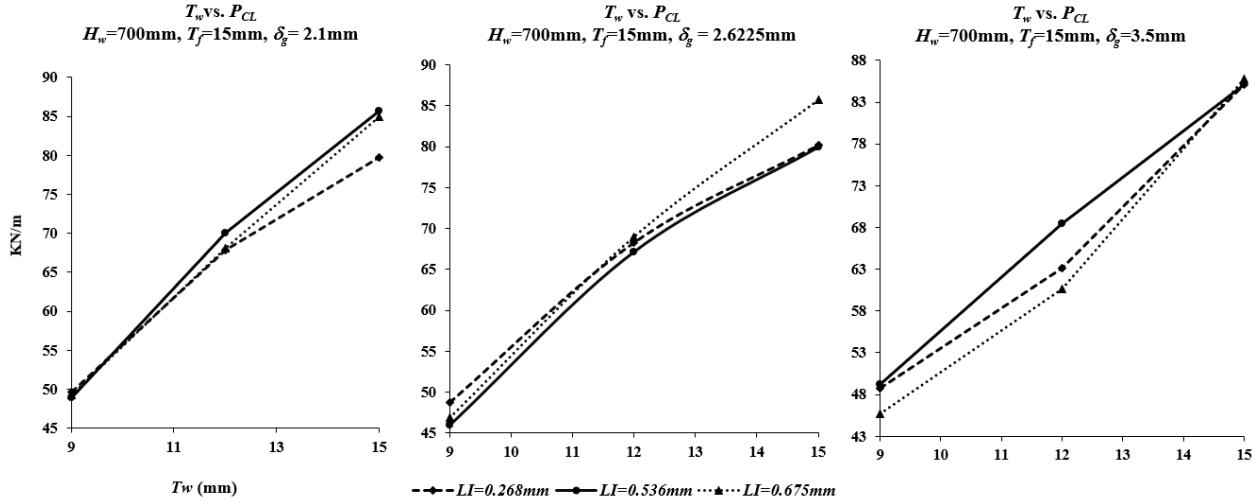
405 Figure 18 displays the effects of varying steel strength class from $S235$ to $S440$ and the variation results in
 406 a significant effect on sections that utilised a larger D_o as the effects were in the region of 17%. However,
 407 for a mid-range opening diameter ($H_w/D_o=1.5$), the effect was approximately 5%. The first graph in Figure
 408 18 ($S235$ and $H_w/D_o=1.7$), demonstrates that the beam collapses at a lower load although the D_o is smaller
 409 compared to the other plots. This particular beam experienced WP buckling ($WP=41\text{mm}$, refer to Table 2)
 410 and stresses at the end WP ($L_{Ed} = 29\text{mm}$) very early in the analysis.



411

412 **Figure 18:** Effects on the steel strength class from S235 (as in Figure 12) to S440

413 Figure 19 represents the effects of the initial geometrical imperfection. The graphs depict the localised and
 414 global imperfection response on the P_{CL} with varying T_w . The effects of the initial imperfection in most
 415 cases were less than 5%. Localised web imperfections, however, seemed to have a slightly higher impact
 416 on the beam response than the global imperfections.



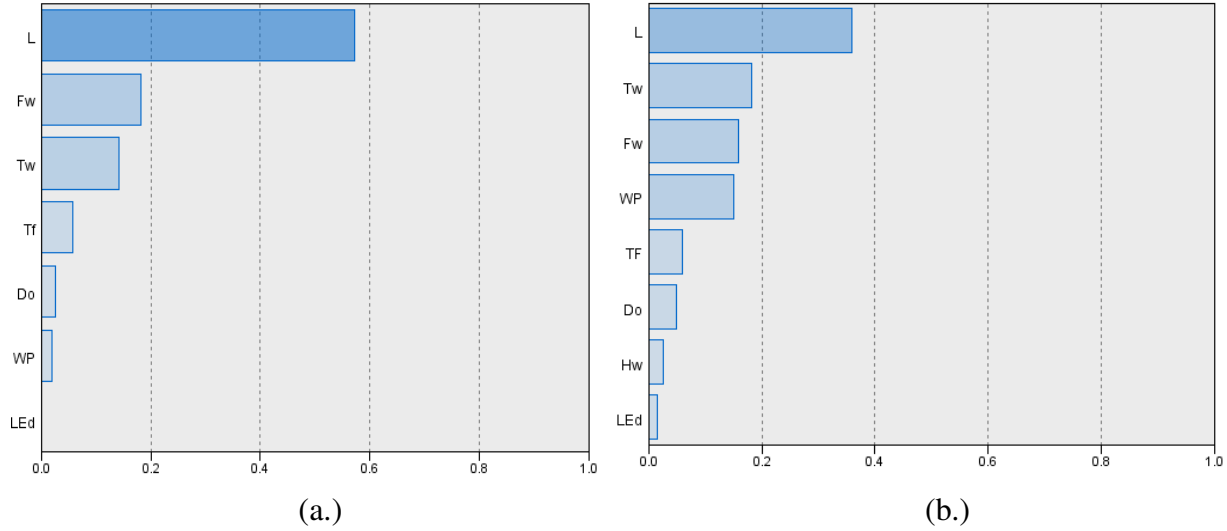
417
 418 **Figure 19:** Effects of the variation of the geometrical imperfection (δ_g and δ_{LI})

419 **5. Global Stepwise Regression (GSR)**

420 Global stepwise regression (GSR) analysis has the potential of producing statistical models to develop a
 421 relationship from a dataset of independent variables to dependent output variables. The process of GSR is
 422 iterative by selecting the best independent variables to represent the regression model (Campbell, 2013).
 423 Therefore, the combination of independent variables that best correlate to the dependent output variable is
 424 identified sequentially by simplifying either adding, deleting or depending on the method to identify which
 425 variable has the greatest impact.

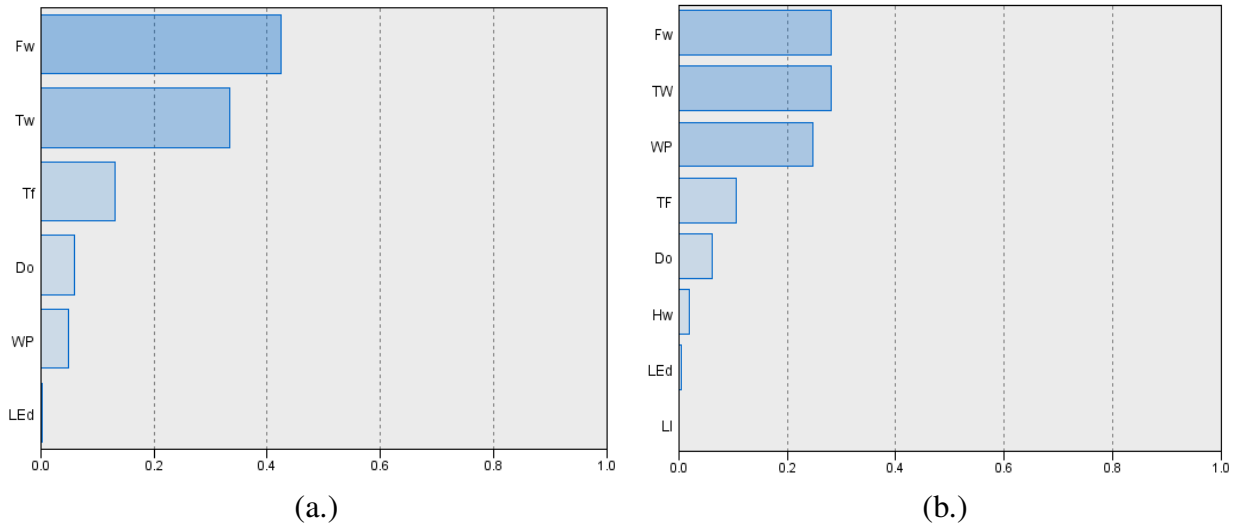
426
 427 Figure 20 highlights the global impact of each parameter on the γ_{cr} and P_{CL} . In Figure 20a, the influences
 428 are L : 57.32%, F_w : 18.1%, T_w : 14.25%, T_f : 5.64%, D_o : 2.58% and L_{Ed} : 0.06%. In Figure 20b, the influences
 429 are L : 35.92%, T_w : 18.29%, F_w : 15.86%, WP : 14.93%, T_f : 5.96%, D_o : 4.98%, H_w : 2.59% and L_{Ed} : 1.47%.

430



431
432
433 **Figure 20:** Important independent parameters impact on (a) γ_{cr} and (b) P_{CL}

434 Figure 21 considers a fixed length of beam to study the influences of each individual parameters globally.
435 The effects of the parameters in Figure 21a for γ_{cr} shows that F_w : 42.38%, T_w : 33.37, T_f : 13.21, D_o : 5.98%,
436 WP : 4.86% and L_{Ed} : 0.19%. Similarly, in Figure 21.b shows the effects of P_{CL} are F_w : 28.18%, T_w : 28.01%,
437 WP : 24.71%, T_f : 10.5%, D_o : 6.1%, H_w :1.92%, L_{Ed} : 0.54% and δ_I :0.04%.



438
439
440 **Figure 21:** Important independent parameters impact on (a) γ_{cr} and (b) P_{CL}

441 **6. Discussion**

442 To summarise, when D_o changes from $H_w/1.25$ to $H_w/1.7$ the γ_{cr} increased by approximately 10.5% for
443 critical members ($5.5 \geq L/H_w \leq 7.5$). Similarly, increasing the WP width from $D_o/10$ to $D_o/2.04$ resulted in
444 an increase in the γ_{cr} by approximately 20.5% and the effect of the D_o becomes trivial. In collapse analysis,
445 when D_o changes from $H_w/1.25$ to $H_w/1.7$ resulted in an increase in the P_{CL} by approximately 20%. Also,
446 changing the web-post width from $D_o/10$ to $D_o/2.04$ resulted in an increase in the P_{CL} by approximately
447 17.5% for slender sections (e.g., $L/H_w = 7.15$ to 9.0). The influence of the load-carrying capacity due to the
448 initial conditions was observed to be lower than 5% for any geometrical imperfection. The influence of the
449 steel yield strength (from $S235$ to $S440$) was approximately 17% but only for the larger diameter

450 ($D_o=H_w/1.25$) of web openings or when $WP=D_o/10$. For any other cases, the influence of the steel yield
451 strength was insignificant.

452

453 In addition, the GSR study demonstrated that γ_{cr} is insensitive ($\approx 5\%$) to a varying perforation geometry
454 but sensitive to the flange (F_w and T_f) and T_w geometry. However, for the collapse analysis, WP influences
455 the P_{CL} greatly at 24.7%. This analysis concludes that the consideration of alternative web opening shapes
456 is possible, without compromising the capacity of the steel perforated beams and similar performances are
457 anticipated overall. Consequently, the work of various researchers on perforated beams with non-standard
458 web opening configurations should be considered for the Eurocode 3 compliance without the need for
459 drastic updates. Similarly, the coherent mass data results generated in this paper can be used to derive
460 sophisticated closed-form solutions. For example, the data has been already used to develop an artificial
461 neural network-based formula (Abambres et al., 2018).

462

463 7. Conclusions

464 From this comprehensive FE investigation, it was concluded that the most critical parameter for both global
465 elastic and inelastic analyses of cellular beams is the web thickness. Since the beams were not laterally
466 restraint, the first buckling mode is a result of the lateral movement of the compression flange, and
467 consequently, both the T_f and F_w had significant impact on the beam response.

468

469 A comparison study was also established between the SCI P355 analytical method and the mass FE data,
470 which demonstrated the level of conservatism of the former. It is also noticeable that the elastic and inelastic
471 FE results are not fluctuating together, with the inelastic analyses comparing very well with the SCI P355
472 calculation which suggests that cellular beams are vastly behaving inelastically, thus design approaches
473 using elastic design should be abandoned.

474

475 Notation

476 The following symbols are used in this paper:

477 D_o : Perforation diameter

478 E : Modulus of Elasticity

479 E_t : Tangential Modulus

480 ε_y : Initial strain of steel

481 ε_f : Final yield strain of steel

482 f_u : Ultimate Stress

483 f_y : Yield stress of steel

484 F_w : Width of flange

485 δ_G : Global geometric imperfection

486 H : Total depth of the member

487 H_w : Height of web (centre of web to web)

488 L : Length of beams

489 L_{Ed} : End web-post distance (end perforation to support)

490 δ_{LI} : Local geometric imperfection

491 $M_R=M_L$: local moment at the perforation

492 M_h : Local moment at the web-post

493 σ_R : Residual stresses

494 P_{CL} : Inelastic collapse load
495 S_o : Center to center of openings.
496 T_f : Flange thickness
497 T_w : Web thickness
498 γ : Material proof stresses of 0.1% and 0.2% in imperfection
499 Y_{cr} : elastic buckling load (N/mm)
500 $V_L = V_R$: Local shear force at the perforation
501 $V_t = V_b$: Local shear force at the top and bottom tee-section.
502 V_h : Local horizontal shear force at the web-post
503 WP: Width of Web post
504 UX , UZ , UY : movement in different plane in model space (Figure 3) UZ : perpendicular to web, UX : along
505 beam and UY : perpendicular to flange.
506 ΔF_{load} : incremental load
507

508 **Data Availability**

509 Both datasets are available at <https://osf.io/5jxut/>
510 For Python scripting contact with corresponding author of the paper at k.tsavdaridis@leeds.ac.uk

512 **References**

- 513 Abambres M, Rajana K, Tsavdaridis KD and Ribeiro T (2018) Neural Network-Based Formula for the
514 Buckling Load Prediction of I-Section Cellular Steel Beams. *Computers*. 8(1), 2.
515 Altfillisch MD, Cooke BR, and Toprac AA (1957) An Investigation of open web expanded beams, *Welding*
516 *Research*, 22(2).
517 Akrami V and Erfani S (2016) Review and assessment of design methodologies for perforated steel beams,
518 *Journal of Structural Engineering*, 142(2), 1-14.
519 American Institute of Steel Construction (2010) Specification for Structural Steel Buildings (ANSI/AISC
520 360-10), American Institute of Steel Construction, Chicago.
521 Bower JE (1968) Design of beams with web openings, *Journal of the Structural Division*, Proceedings of
522 the American Society of Civil Engineers, 94(3), 783-808.
523 Bradford MA (1992) Lateral-distortional buckling of steel I-section members, *Journal of Constructional*
524 *Steel Research*, 23(1-3), 97-116.
525 Bradford MA (1998) Distortional buckling of elastically restrained cantilevers, *Journal of Constructional*
526 *Steel Research*, 47(1-2), 3-18.
527 Campbell M (2013) *Statistics at Square Two*. New York, NY: John Wiley & Sons.
528 London: GBR: BMJ Publishing Group.
529 Chung K F, Liu TCH and Ko ACH (2001) Investigation on Vierendeel mechanism in steel beams with
530 circular web openings. *Journal of Constructional Steel Research*, 57, 467-490.
531 Chung KF, Liu CH and Ko ACH (2003) Steel beams with large web openings of various shapes and sizes:
532 an empirical design method using a generalized moment-shear interaction curve, *Journal of Construction*
533 *Steel Research*, 59(9), 1177-1200.
534 Clawson WC and Darwin D (1980) *Composite beams with web openings*, Kansas State University, Kansas.

535 Darwin D (1990). Steel and composite beams with web opening, *Steel Design Guide Series 2*, AISC,
536 Chicago.

537 Dassault Systèmes (2011) ABAQUS 6.11, Abaqus/CAE user's manual, Dassault Systems, USA.

538 Dassault Systèmes Simulia Corp (2017). ABAQUS CAE (2017). [Software].

539 Dawson RG and Walker AC (1972). Post-buckling of geometrically imperfect plates, *Journal of Structural*
540 *Engineering*, 98(1), 75-94.

541 Ellobody E (2011) Interaction of buckling modes in castellated steel beams, *Journal of Constructional Steel*
542 *Research*, 67(2011), 814-825.

543 Ellobody E (2012) Nonlinear analysis of cellular steel beams under combined buckling modes, *Thin-Walled*
544 *Structures*, 52, 66-79.

545 Ellobody E (2017). Interaction of buckling modes in railway plate girder steel bridges, *Thin-Walled*
546 *Structures*, 115, 58-75.

547 Gardner L and Nethercot DA (2004) Numerical modelling of stainless-steel structural components- A
548 consistent approach, *Journal of Structural Engineering*, 130(10), 1586-1601.

549 Hesham Martini MIM (2011) Elasto-plastic lateral torsional buckling of steel beams with perforated web,
550 Ph.D. Thesis, United Arab Emirates University.

551 Hosain MU and Speirs WG (1971) Failure of castellated beams due to rupture of welded joints, *Acier-*
552 *Stahl-Steel*, 36(1), 34-40.

553 Kerdal D and Nethercot DA (1984) Failure modes for castellated beams, *Journal of Constructional Steel*
554 *Research*, 4(1984), 295-315.

555 Kingman JJ, Tsavdaridis KD and Toropov VV (2015) Applications of Topology Optimisation in Structural
556 Engineering: High-rise Buildings & Steel Components, *Jordan Journal of Civil Engineering*, 9(3), 335-
557 357.

558 Kolosowski J (1964) Stresses and deflections in castellated beams, *The Structural Engineer*, 42 (1).

559 Kwani S and Wijaya PK (2017). Lateral torsional buckling of castellated beams analysed using the collapse
560 analysis, *Procedia Engineering*, 171(2017), 813-820.

561 Lawson RM (1987) Design for openings in the webs of composite beams SCI P068. Steel Construction
562 Institute, Berkshire, UK.

563 Lawson RM and Hicks SJ (2011) Design of composite beams with large openings SCI P355. Steel
564 Construction Institute, Berkshire, UK.

565 Lucas WK and Darwin D (1990) Steel and composite beams with web openings. The American Iron and
566 Steel Institute, Kansas.

567 Maraveas C, Tsavdaridis KD and Nadjai A (2017) Fire Resistance of Partially Unprotected Ultra Shallow
568 Floor Beams (USFB): A Numerical Investigation, *Fire Technology*, 53(2), 609-627.

569 Redwood RG and McCuthcheon JO (1968) Beam tests with unreinforced web openings, *Journal of the*
570 *Structural Division*, 94, 1-17.

571 Redwood RG, Baranda H and Daly MJ (1978) Tests of thin-webbed beams with unreinforced holes, *Journal*
572 *of the Structural Division*, 104(3), 577-595.

573 Sweedan A (2011) Elastic lateral stability of I-shaped cellular steel beams. *Journal of Constructional Steel*
574 *Research*, 67(2), 151-163.

575 SEI/ASCE (1998) Specifications for structural steel beams with openings, SEI/ASCE 23-97, ASCE, Reston
576 VA.

577 Sonck D (2014). Global buckling of castellated and cellular steel beams and columns, Ph.D. Thesis, Ghent
578 University.

579 Surtees JO and Lui Z (1995) Report of loading tests on cellform beams. Research Report, University of
580 Leeds, Leeds.

581 Taras A (2010) Contribution to the Development of Consistent Stability Design Rules for Steel Members.
582 Phd thesis, Graz University of Technology

583 Toprac AA and Cooke BR (1959) An experimental investigation of open-web beams, Welding Research
584 Council, New York.

585 Tsavdaridis KD (2010) Structural performance of perforated steel beams with novel web openings and with
586 partial concrete encasement, Ph.D. Thesis, City University London.

587 Tsavdaridis KD and D'Mello C (2009) Finite Element Investigation of Perforated Beams with Different
588 Web Opening Configurations. The 6th International Conference on Advances in Steel Structures (ICASS
589 2009). 16-18 December 2009, Hong Kong, China, 213-220.

590 Tsavdaridis KD and D'Mello C (2011) Web buckling study of the behaviour and strength of perforated steel
591 beams with different novel web opening shapes. *Journal of Constructional Steel Research*, 67 (10), 1605-
592 20.

593 Tsavdaridis KD and D'Mello C (2012) Vierendeel bending study of perforated steel beams with various
594 novel web opening shapes through non-linear finite element analyses. *Journal of Structural Engineering*,
595 138 (10), 1214- 30.

596 Tsavdaridis KD, D'Mello C and Huo BY (2013) Experimental and Computational Study of Vertical Shear
597 Behaviour of Partially Encased Perforated Steel Beams. *Engineering Structures*. 56, 805-822.

598 Tsavdaridis KD and Galiatsatos G (2015) Assessment of Cellular Beams with Transverse Stiffeners and
599 Closely Spaced Web Openings. *Thin-Walled Structures*. 94, 636-650.

600 Verweij JG (2010) Cellular beam-columns in portal frame structures. MSc. Thesis, Delft University of
601 Technology, Holland.

602 Huo BY, D'Mello C and Tsavdaridis KD (2010) Experimental and Analytical Study of Push-out Shear
603 Tests in Ultra Shallow Floor Beams. The 34th International Association for Bridge and Structural
604 Engineering Symposium (IABSE 2010). 22-24 September 2010, Venice, Italy, IABSE Proceedings, 31-38.

605 Ward JK (1990) Design of composite and non-composite cellular beams SCI P100. Steel Construction
606 Institute, Berkshire, UK.

607 Zirakian T and Showkati H (2006) Distortional buckling of castellated beams, *Journal of Constructional*
608 *Steel Research*, 62(9), 863-871.

609 Zirakian T (2008) Elastic distortional buckling of doubly symmetric I-shaped flexural members with
610 slender webs, *Thin-Walled Structures*, 46(5), 466-475.